Additive manufacturing of an electrically triggered actuator: electro-thermo-mechanical behaviour of a carbon black/polylactic acid composite.

Laurane Roumy, Thuy Quynh Truong Hoang, Damien Marchand, Fabienne Touchard, Francisca Martinez-Hergueta

ADDITIVE MANUFACTURING OF AN ELECTRICALLY TRIGGERED ACTUATOR: ELECTRO-THERMO-MECHANICAL BEHAVIOUR OF A CARBON BLACK/POLYLACTIC ACID COMPOSITE

L. Roumy[1,2,3], T-Q. Truong-Hoang[2], D. Marchand[1], F. Touchard[1], F. Martinez-Hergueta[3]

[1]Institut Pprime, CNRS-ENSMA-Université de Poitiers, Département Physique et Mécanique des Matériaux, ENSMA, 1 Av. C. Ader, B.P. 40109, 86961 Futuroscope Cedex, France
Email: laurane.roumy@ensma.fr, damien.marchand@ensma.fr, fabienne.touchard@ensma.fr
[2]ESTACA, ESTACA'Lab-Laval, F53000 Laval, France
Email: thuy-quynh.truong-hoang@estaca.fr
[3]School of Engineering, Institute for Infrastructure and Environment, University of Edinburgh, UK
Email: francisca.mhergueta@ed.ac.uk

Keywords: 4D printing, monotonic tensile test, Joule effect, multifunctional hinge, shape memory polymer

Abstract
Four dimensional (4D) printing is a process that consists of the additive manufacturing of smart materials. Polylactic acid (PLA) is a thermosensitive shape memory polymer that can shift shape when heated above its glass transition temperature and that is commonly used in Fused Filament Fabrication (FFF). Once filled with carbon black (CB) particles, CB/PLA can be 3D printed and electrically heated by Joule effect, giving the possibility of remotely electrically triggered structures. However, this material raises multiple questions, such as its electro-thermo-mechanical coupling. In this study, CB/PLA samples undergo monotonic tensile loading to better understand the influence of the printing direction on the electro-mechanical properties of three dimensional (3D) printed samples. In addition, the resistivity of the samples is measured throughout the tensile tests. Results show that the printing direction highly influences the mechanical and electrical properties, highlighting the superior properties of the 0° samples. The conclusions drawn by this study underline the interest in using the longitudinal and unidirectional printing direction to improve the conductive path within the samples, therefore leading to the manufacturing of a hinge able to recover more than 90% of its initial shape.

1. Introduction

Four dimensional (4D) printing combines additive manufacturing with a smart material, time being the fourth dimension. Shape Memory Polymers (SMP) are often used because of their ability to shift shape to a pre-programmed configuration under an external stimulus. This way, a movement can be created without any motors or human action. This technology finds applications in soft robotics, medicine, and space exploration for instance [1]. Amongst various 3D printing techniques, Fused Filament Fabrication (FFF) is commonly used to manufacture 4D printed devices with SMPs [2]. In particular, conductive carbon black (CB) reinforced polymers that can heat through the Joule effect are of great interest for 4D printing. This kind of materials allows remote electrical actuation of devices. Polylactic acid (PLA) is a bio-sourced thermoplastic Shape Memory Polymer commonly used in FFF. When filled with CB, it becomes an electrosensitive material.

In a previous article, the effects of the printing parameters on the electro-thermal properties of 3D printed carbon black/polylactic acid (CB/PLA) composites were determined [3]. In terms of electro-mechanical coupling, to the author's knowledge, only a few studies partially considered the question for 3D printed

CB/PLA specimens. Tirado-Garcia et al. [4] studied the evolution of the electrical resistance during a tensile test of a 0° sample, whose filaments are printed along the longitudinal direction, which is the same as the loading direction. Yet, no other printing direction is considered. Crespo-Miguel et al. [5] carried out tensile tests on the same raster angles after being subjected to several voltages as an electro-mechanical coupling, but no monitoring of the resistance throughout the experiment was performed. In relation to the thermo-mechanical coupling, they studied different raster angles under tensile testing in environmental chambers to analyse the effect of various temperatures on the material's behaviour. However, Delbart et al. [6] compared the effects of oven heating and Joule heating on CB/PLA samples, and demonstrated noticeable differences between the two techniques as a result of the different thermal inertia induced. It shows the limits of using environmental chambers to characterise the governing electro-thermal equations when using the Joule effect.

The aim of this study is to gain a better understanding of the electrical, mechanical and thermal coupling in the 3D printed CB/PLA and develop a prototype of 4D printed hinge. Rectangular samples of CB/PLA composites were 3D printed with different raster angles and stacking sequences. Multi-instrumented tensile tests were then performed to measure the mechanical properties and electrical resistance evolution of the specimens. An actuator prototype was then designed by printing a composite structure with the filaments aligned along the electricity path.

2. Materials and methods

2.1. CB/PLA and manufacturing method

In this study, the material considered is the Proto Pasta's electrically conductive composite PLA that consists of polylactic acid filled with carbon black particles (CB/PLA). Ultimaker printers with the Fused Filament Fabrication technology were used with a nozzle of 0.8mm of diameter heated at 210°C. The sample was 3D modelled thanks to the CAD software CATIA V5 to obtain an .stl file that was converted to a .gcode file thanks to Ultimaker Cura. This software was used to define the printing parameters and the path followed by the printer. The samples were printed with an infill density of 100% and a printing speed of 60mm/s. The parameters of the filaments were set to a layer height of 0.1mm, a line width of 0.7mm and deposited on a bed heated at 60°C. These parameters were optimised in a previous work [3].

2.2. Multi-instrumented tensile test

Rectangular samples were manufactured following the standard test method for tensile properties of polymer matrix composite materials ASTM D 3039/3039M. Their dimensions were 175x20x3mm^3 and rectangular glass/epoxy tabs with a dimension of 40x20x1.5mm^3 were glued on the samples with Araldite epoxy resin (Figure 1). Three raster angles were studied: 0° filaments following the longitudinal length of the sample; 90° filaments that are perpendicular to this direction; and ±45° filaments that consist of an alternation of layers that are at ±45° compared to the longitudinal direction. Each sample consists of several layers with the same printing directions. A quasi-isotropic (QI) sample with a $[0_6/\pm45_5/90_5]_S$ stacking sequence was also manufactured. In order to measure the electrical resistance of the samples, silver paint was applied at the two extremities of their cross-section and wires were glued with Araldite epoxy resin.

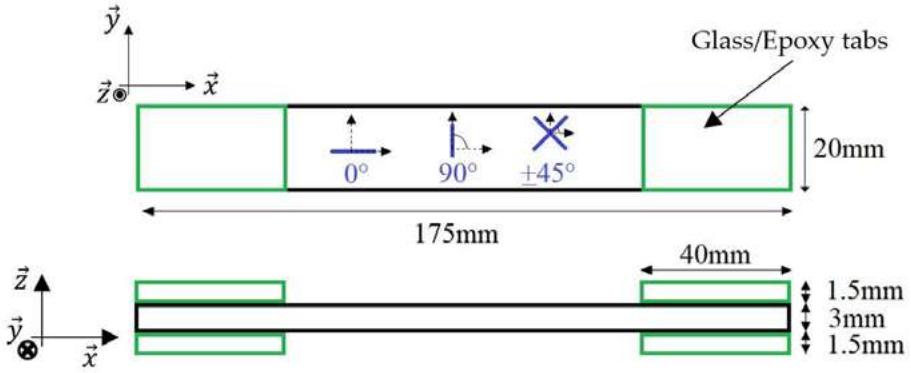

Figure 1. Dimensions of the rectangular tensile samples with the different raster angles.

Monotonic tensile tests were conducted at a cross-head speed of 1mm/min, the load was applied along the $\vec{x}$ axis of the samples (Figure 1). The rectangular specimens were clamped in a 5982 Instron machine (Figure 2(a)) and instrumented with longitudinal and transverse extensometers to measure the corresponding strains (Figure 2(b)). A longitudinal gauge length of 50mm was used. The sample was also connected to a 2-point probe MTX 3250 multimetre that measured the electrical resistance of the samples during the tests. Seven to ten specimens were tested for each lay-up studied.

The electrical resistance *R(t)* measured during the tensile tests depends on the length *L(t)* and cross-section area *S(t)* of the sample at time t. To remove this dependency, the resistivity *ρ(t)*, which is inherent to the material, was considered with the formula [7] (Eq.1):

$$\rho(t) = \frac{R(t).S(t)}{L(t)}, \tag{1}$$

The hypothesis that the Poisson's ratio ν is the same in directions xy and xz was made (Eq.2):

$$\nu_{xy} = \nu_{xz}. \tag{2}$$

Therefore, the transverse and out-of-plane strains, respectively $\varepsilon_{yy}(t)$ and $\varepsilon_{zz}(t)$, were considered equal all along the experiment (Eq.3):

$$\varepsilon_{yy}(t) = \varepsilon_{zz}(t). \tag{3}$$

The section *S(t)* at any time could then be deduced (Eq.4):

$$S(t) = S_0(1 + \varepsilon_{yy}(t))^2, \tag{4}$$

with S_0 the initial cross-section of the sample. In addition, the evolution of the length of the sample *L(t)* depends on the length of the tabs L_T, the initial total length of the sample L_0 and the longitudinal strain $\varepsilon_{xx}(t)$ (Eq.5):

$$L(t) = L_T + (L_0 - L_T).(1 + \varepsilon_{xx}(t)). \tag{5}$$

This way, the resistivity *ρ(t)* of the sample could be calculated throughout the tensile test (Eq.6):

$$\rho(t) = \frac{R(t).S_0(1+\varepsilon_{yy}(t))^2}{L_T+(L_0-L_T).(1+\varepsilon_{xx}(t))}, \tag{6}$$

with *R(t)* the measured electrical resistance, L_0 and S_0 the initial length and cross-section of the sample respectively, L_T the length of the tabs, $\varepsilon_{xx}(t)$ and $\varepsilon_{yy}(t)$ the longitudinal and transverse strains measured by the extensometers respectively.

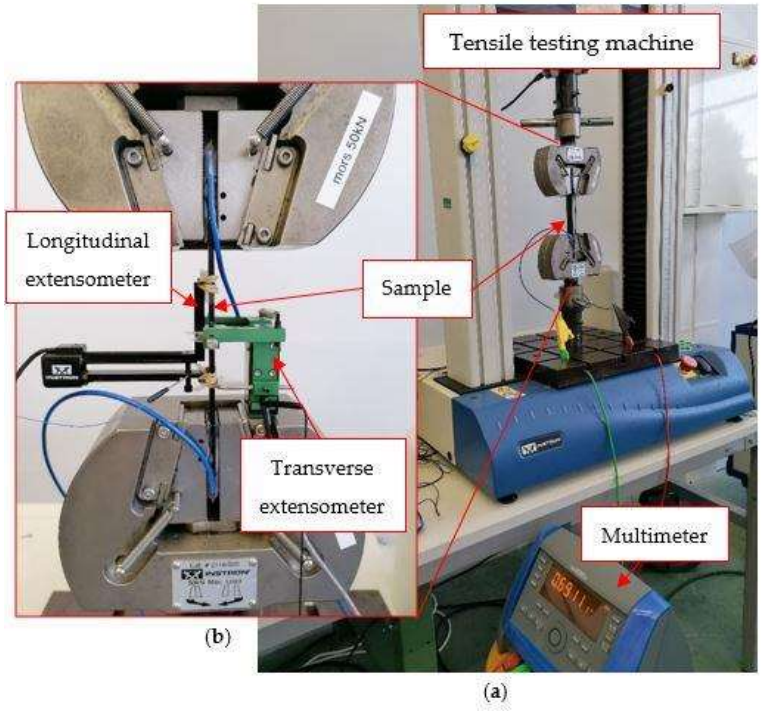

Figure 2. (**a**) Setup for the measurement of the electrical resistance during tensile tests. (**b**) Focus on the sample and the measurement of the longitudinal and transverse strains.

2.3. Damage observation

For microstructural observations, the samples were sputtered with a thin layer of gold before using a VEGA3 TESCAN scanning electron microscope (SEM) with secondary electrons accelerated with a voltage of 10 kV.

2.4. Design of a hinge

The principle of the hinge developed in this article is to manufacture a structure that can be folded at a 90° angle and be deployed to come back to a 0° angle. Since the material shape memory behaviour is electro activated, the design was thought so that the electrical input and output would be on the same line. An omega shape structure of 1mm of thickness was therefore designed and inspired from Liu et al. work [8] (Figure 3).

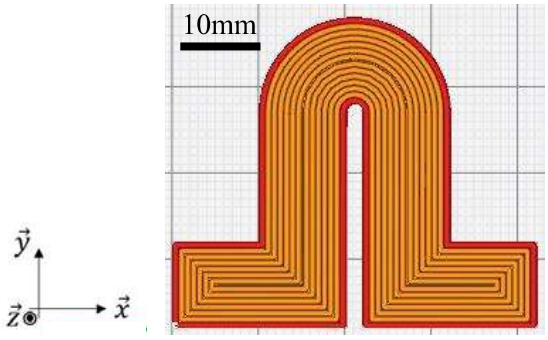

Figure 3. Ultimaker Cura view of the designed hinge.

To obtain the lowest electrical resistance, it was demonstrated in a previous article that the printed filaments should follow the path of the electricity as designed in Figure 3 [3].

3. Results and discussion

3.1. Mechanical properties and evolution of the resistivity

A mechanical characterisation of 3D printed CB/PLA samples was conducted. The mechanical properties measured are summarised in Table 1. The highest Young's modulus of 2542 MPa is obtained for the 0° sample and the lowest at 1744 MPa is for the 90° sample. The quasi-isotropic sample has a stiffness of 2187 MPa similar to the ±45° sample with a stiffness of 2108 MPa. Regarding the Poisson's ratio, the values decrease slowly from 0.42 for a 0° sample, to 0.40 for a ±45° sample and 0.37 for a quasi-isotropic sample. The 90° samples have a fairly lower Poisson's ratio equal to 0.25 which means that this kind of sample is less compressible than the others. It is explained by the fact that the stiffness of the filaments acts against the decrease of their length in the transverse direction of the 90° specimens. In terms of the maximum stress, failure stress and elongation at break, the results show the poor mechanical properties of the 90° specimens compared to the other raster angles. This is explained by the weakness of the inter-filament interface that endures the stress, which causes the failure stress to decrease in this structure, where for the other printing directions, the filaments take the stress over. The QI samples present a higher maximum stress and failure stress than the ±45° samples, but a lower elongation at break. It can be explained by two coupled mechanisms: the weakening of the structure by the 90° layers and the strengthening due to the 0° layers. Overall, the 0° specimens have much better mechanical properties than the other raster angles.

Table 1. Mechanical properties.

Raster angle	Young's modulus (MPa)	Poisson's ratio	Maximum stress (MPa)	Failure stress (MPa)	Elongation at break (%)
0°	2542 ± 15	0.42 ± 0.03	29.6 ± 1.7	26.8 ± 2.0	3.47 ± 0.39
±45°	2108 ± 86	0.40 ± 0.03	19.6 ± 2.3	18.7 ± 2.5	2.36 ± 0.15
90°	1744 ± 108	0.25 ± 0.01	8.3 ± 0.9	7.8 ± 1.2	0.70 ± 0.07
QI	2187 ± 125	0.37 ± 0.05	21.8 ± 0.8	21.7 ±0.7	1.89 ± 0.13

An example of the stress-strain curve of the 0° specimen is presented in Figure 4 (red dots). An SEM image of the fracture surface of the sample shows that the failure is due to filaments breaking, but not all in the same plane, resulting in partial debonding from one filament to another between two superimposed layers (Figure 4). The evolution of the resistivity calculated thanks to Eq. 6 is then analysed (blue triangles). Three different stages can be observed: an increase in resistivity when the

sample is in its elastic domain (first stage); a decrease of the resistivity between the beginning of the plastic domain and the reaching of the maximum stress (second stage); and finally a huge increase in resistivity up to the failure of the sample (third stage). This behaviour has already been observed and a hypothesis of explanation was suggested by Tirado-Garcia et al. [4]. In the initial state of the sample, electrical pathways are created between the carbon black particles. These paths can be within a filament or between two adjacent filaments, but the interface between the filaments makes it harder for the electricity to propagate. Therefore, the electricity always chooses the easiest path, most likely mainly propagating within a filament when possible. In the first stage of the tensile test, the distance between the particles increases as the sample has an elastic behaviour and its length increases. It results in a slow increase in resistivity as the paths between some particles might be suppressed due to the distance between them being too high, but the majority of the pathways is maintained. Once the sample enters its plastic behaviour in the second stage, the particles are brought together in the vertical dimension due to the Poisson effect influence. It is traduced by reducing the transverse dimension while the longitudinal dimension still increases. This phenomenon creates new paths for the electrons within a filament and between them as the interparticle distance decreases, leading to an increase in the conductivity overall. This trend reverses in the third stage once the maximum stress is reached, as the interparticle distance is too high and the development of crazes prevents the electricity from circulating, leading to the progressive destruction of electrical pathways, finally shooting up shortly before failure.

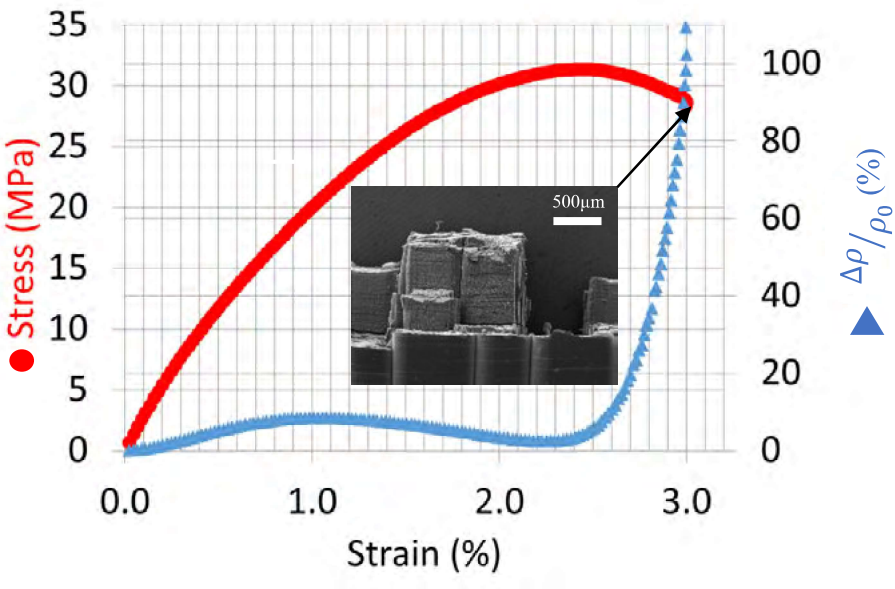

Figure 4. Stress-strain curve coupled with the evolution of the relative variation of resistivity for a longitudinal 3D printed CB/PLA composite sample and SEM image of the fracture surface.

The study of the mechanical properties, as well as the electrical properties of the different raster angles and stacking sequences, highlights the interest in using a unidirectional and longitudinal printing path to deposit the melted filaments during the 3D printing process. Indeed, the 0° samples have better mechanical and electrical properties than their 90°, ±45° and QI counterparts [9].

3.2. 4D printing process

To take advantage of the better mechanical and electrical properties of longitudinal and unidirectional samples, the hinge was manufactured with the printing filaments deposited parallel to the electricity path (Figure 3). Then, to perform the 4D printing process, two steps are involved. A programming step where the hinge is heated by Joule effect at 50V above its glass transition temperature and folded to a 90° angle, which is its temporary shape. The sample is then cooled down while the temporary shape is held

(Figure 5(a)). Once cold, the hinge is heated again at 50V for the triggering step and the shape memory effect applies, leading to the actuation of the deployment of the sample (Figure 5(b)). The hinge recovers its permanent shape which is the shape it has after 3D printing, a 0° angle (Figure 5(c)).

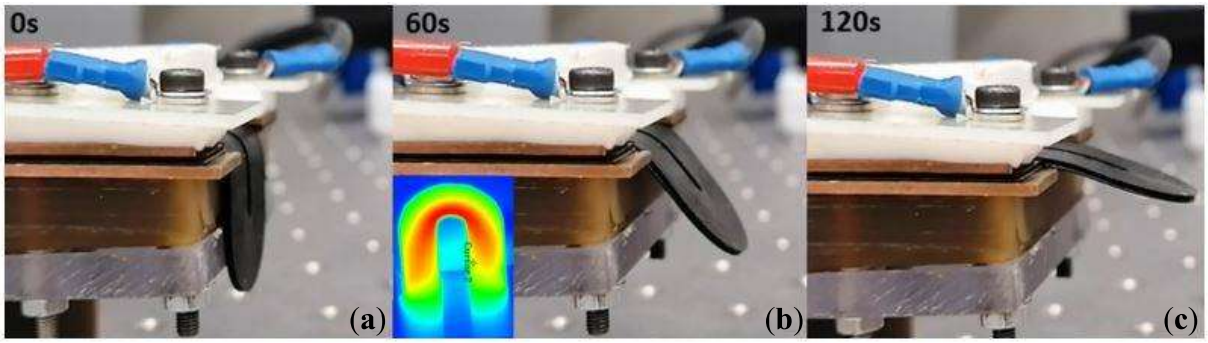

Figure 5. Snap shots of the deployment of an electro activated CB/PLA hinge recovering its initial flat shape with thermal camera temperature measurements during actuation.

The hinge's recovery ratio was calculated by comparing the angle after the shape recovery to the initial one. The folding process significantly impacts the recovery ratio. Several techniques were used, and Figure 6 shows the corresponding recovery ratios measured. The main difference between the two methods is the control of the Joule heating with the voltage. In the first method, the samples were heated at a temperature that was too high above their glass transition temperature and damage such as the shrinking of the transverse direction, or failure at the joints of the hinge were witnessed. In addition, a tool to help the folding of the sample and achieve a reproducible angle during the programming step was 3D printed in acrylonitrile butadiene styrene for the method two. As a result, the second row of trials more than doubles the first one, showing that a recovery ratio of more than 90% can be obtained.

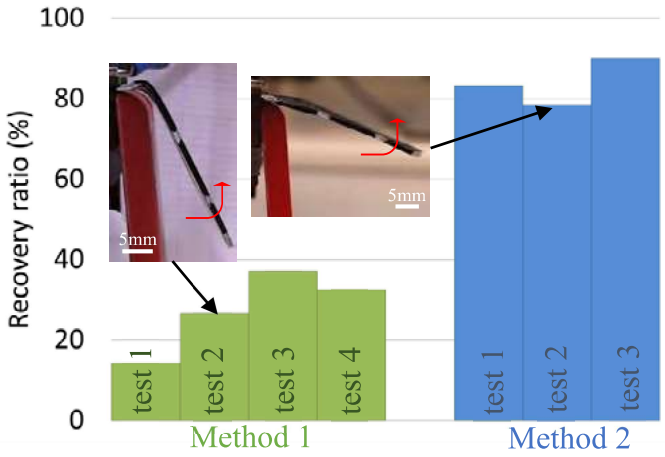

Figure 6. Evolution of the recovery ratio with the methods of programming step and shape of the actuator after the triggering step.

4. Conclusion

In this paper, an electro-thermo-mechanical study of 3D printed CB/PLA samples as well as the design of a 4D printed hinge was presented. First, rectangular shaped samples with different raster angles and stacking sequences were manufactured to measure the mechanical properties by monotonic tensile test depending on the printing direction. Results showed the superior properties of 0° samples, whose

filaments are printed along the longitudinal loading direction. The measurement of the electrical resistance throughout the tensile test highlighted the complex evolution of the resistivity that can be described in three stages. The choice of using a longitudinal unidirectional printing path was then made to design an omega shaped electro activated hinge. Different folding methods to obtain the best recovery ratio with the programming of a 90° angle were studied, leading to more than 90% of recovery ratio. In conclusion, this study contributes to the understanding of electro-thermo-mechanical coupling of an electrically triggered thermosensitive SMP. Furthermore, the application of this material as an electro activated hinge able to perform a 90° deployment is demonstrated. Future work on the study of the durability and the improvement of the recovery ratio of the hinge is considered.

Acknowledgements
This works was supported by the Defence Innovation Agency (AID) of the French Ministry of the Armed Forces through the grant [AID-2021 65 0045].

References
[1] A. Mitchell, U. Lafont, M. Hołyńska, and C. Semprimoschnig, 'Additive manufacturing — A review of 4D printing and future applications', *Additive Manufacturing*, vol. 24, pp. 606–626, Dec. 2018, doi: 10.1016/j.addma.2018.10.038.
[2] A. Kafle, E. Luis, R. Silwal, H. M. Pan, P. L. Shrestha, and A. K. Bastola, '3D/4D Printing of Polymers: Fused Deposition Modelling (FDM), Selective Laser Sintering (SLS), and Stereolithography (SLA)', *Polymers*, vol. 13, no. 18, Art. no. 18, Jan. 2021, doi: 10.3390/polym13183101.
[3] L. Roumy, F. Touchard, D. Marchand, T. Q. Truong Hoang, and F. Martinez-Hergueta, 'Durability of Joule effect of 3D printed carbon black/polylactic acid: Electrical cyclic tests and analytical modelling', *International Journal of Fatigue*, vol. 173, p. 107677, Aug. 2023, doi: 10.1016/j.ijfatigue.2023.107677.
[4] I. Tirado-Garcia *et al.*, 'Conductive 3D printed PLA composites: On the interplay of mechanical, electrical and thermal behaviours', *Composite Structures*, vol. 265, p. 113744, Jun. 2021, doi: 10.1016/j.compstruct.2021.113744.
[5] J. Crespo-Miguel, D. Garcia-Gonzalez, G. Robles, M. Hossain, J. M. Martinez-Tarifa, and A. Arias, 'Thermo-electro-mechanical aging and degradation of conductive 3D printed PLA/CB composite', *Composite Structures*, vol. 316, p. 116992, Jul. 2023, doi: 10.1016/j.compstruct.2023.116992.
[6] R. Delbart *et al.*, 'Multiscale characterisation of the electrical response of 3d printed carbon black polylactic acid', *J Mater Sci*, vol. 58, no. 32, pp. 13118–13135, Aug. 2023, doi: 10.1007/s10853-023-08840-6.
[7] K. Hamdi, Z. Aboura, W. Harizi, and K. Khellil, 'Structural health monitoring of carbon fiber reinforced matrix by the resistance variation method', *Journal of Composite Materials*, vol. 54, no. 25, pp. 3919–3930, Oct. 2020, doi: 10.1177/0021998320921476.
[8] Y. Liu *et al.*, 'Remotely and Sequentially Controlled Actuation of Electroactivated Carbon Nanotube/Shape Memory Polymer Composites', *Adv. Mater. Technol.*, vol. 4, no. 12, p. 1900600, Dec. 2019, doi: 10.1002/admt.201900600.
[9] L. Roumy, T.-Q. Truong-Hoang, F. Touchard, C. Robert, and F. Martinez-Hergueta, 'Electro-Mechanical Characterisation and Damage Monitoring by Acoustic Emission of 3D-Printed CB/PLA', *Materials*, vol. 17, no. 5, p. 1047, Feb. 2024, doi: 10.3390/ma17051047.